JOURNAL OF MATERIALS SCIENCE 30 (1995) 1921–1930

Pre-induction and induction hydration of tricalcium silicate: an environmental scanning electron microscopy study

P. MEREDITH, A. M. DONALD
Polymer and Colloids Group, Cavendish Laboratory, Cambridge University Physics Department, Madingley Road, Cambridge CB3 0HE, UK

K. LUKE
Schlumberger Cambridge Research, High Cross, Madingley Road, Cambridge, UK

Environmental scanning electron microscopy (ESEM) has been used to study the very early pre-induction, and induction physical processes that occur in the hydration of tricalcium silicate. An *in situ* experimental technique is described which allows direct, real-time observation of the sub-micrometre morphological changes that take place during this reaction. The results of this investigation are correlated with kinetic data obtained by differential scanning calorimetry (DSC). In this way, microstructural evolution has been identified with the stages of very early hydration. Upon first contact with water, a gelatinous coating was seen to form at grain surfaces and a crystalline secondary product was observed at the end of an extensive dormant period. These findings are viewed in the light of previous "wet" and "dry" microscopy studies, and are discussed within the framework of ordinary Portland cement as a possible explanation of induction. Comment is made as to the suitability of environmental SEM for analysis of such materials.

1. Introduction

1.1. Tricalcium silicate and ordinary Portland cement

Tricalcium silicate, commonly known as alite, is one of the major components in ordinary Portland cement (OPC). Formulations differ, but in common mixtures the compound forms approximately 50% of the composite. In cement nomenclature, tricalcium silicate is given the symbol C_3S: together with tricalcium aluminate (C_3A), dicalcium silicate (C_2S), tetracalcium aluminoferrite (C_4AF), and gypsum ($C\bar{S}H_2$), it forms a complex multiphase system. For a detailed account of cement chemistry the reader is directed towards one of the numerous texts on the subject, see, for example, Taylor [1].

OPC is manufactured by firing a mixture of limestone and clay or shale. The "clinker" that is formed is then ground with gypsum to form a fine powder containing multiphase grains in the size range 1–100 μm. Cement enjoys extensive use in the building, engineering and oil industries and remains today one of the most important materials in our modern society. Given such widespread use, it is rather surprising that the way in which cement reacts with water is not fully understood. The explanation of this fact lies in the complex chemical and physical processes which underpin its transformation, via hydration, from a dry powder to a strong, porous solid.

The hardening process is thought to be principally associated with the silicate-phase reaction products. The hydration of tricalcium silicate follows the approximate reaction scheme

$$\underset{\text{tricalcium silicate}}{C_3S} + \underset{\text{water}}{(y+z)H} \rightarrow \underset{\substack{\text{hydrated calcium silicate} \\ \text{(C–S–H)}}}{C_xSH_y} + \underset{\text{calcium hydroxide}}{zCH} \quad (1)$$

where $x + z = 3$, but x, y, z are not necessarily integers.

Hydrated calcium silicate (C–S–H) is the major product, and its stoichiometry, as is evident from the above equation, may vary over a large compositional range [2]. The compound, which was originally called tobermorite gel, exhibits very poor crystallinity [3]. It is known to have a variety of morphological forms associated with different stages of the reaction. For example, during the early part of hydration, C–S–H has an ill-defined amorphous microstructure, whilst at later stages it is seen to form into long interpenetrating hollow fibrils [4]. In hydrated OPC, C–S–H makes up approximately 70% of the total volume, and forms the binding agent between unreacted grains and more crystalline phases [5]. The second reactant product, calcium hydroxide (CH), is of a fixed composition and displays a high degree of crystallinity [3]. It forms distinctive hexagonal plates of material during the later stages of the reaction, which can grow until visible by the naked eye [6]. The hydration of the other silicate phase, C_2S or belite, proceeds in a very

0022–2461

similar manner. Its kinetics are, however, much retarded, and the long-term hardening of cement over many months or even years is associated with this compound [4].

A popular method for investigating the hydration kinetics of cement and isolated components such as C_3S, has been conduction calorimetry [7]. The technique involves an isothermal measurement of the amount of heat evolved during a reaction as a function of time. Numerous sets of results [3, 4, 8, 9] have shown that the hydration mechanism of cement has a series of distinct stages. Immediately following the addition of water, a large amount of heat is given out as ions are liberated into solution from the grain surfaces (stage 1). This rate falls off after ~ 15–30 min and the reaction enters a so-called dormant or induction phase which lasts for several hours (stage 2). At the beginning of stage 3 the hydration begins once more. The reaction peaks at between 10 and 16 h. before falling off again during stage 4 and attaining a long-term equilibrium when the final set and hardening of stage 5 occurs. Fig. 1a shows schematically the trend of this process for the case of OPC hydration.

Forrester [7] argues that much of the heat evolved during stage 3 of the reaction can be attributed to the hydration of C_3S and the formation of C–S–H. Indeed, Kondu and Ueda [10] published quantitative results which showed that the reaction of this component in isolation gave very similar kinetic trends (Fig. 1b). Such data suggest that a further understanding of the cement hydration process can be gained by studying the much simpler silicate systems.

1.2. Product microstructure

The important reactions that take place during these hydration sequences (C_3S and OPC) are thought to occur in a topochemical fashion at the grain surfaces [4, 11–15]. In this mechanism, reaction products are formed in the near vicinity of the source of ion dissolution. It had previously been argued that the mechanism was of the through-solution type, whereby the dissolution and precipitation processes involve long-range transport through the bulk aqueous phase [16, 17]. The development of electron microscopy has allowed the direct observation of grain and product morphology, and the local product theories have recently found more favour with the cement community.

Scanning and transmission electron microscopy have been well used tools in microstructural investigations of cement-like materials. Numerous publications exist on SEM characterization of tricalcium silicate [5, 13, 18–20] and of OPC [8, 21–24]. Scanning transmission and transmission electron microscopy (STEM: TEM studies with their higher resolutions) are less abundant [25–28], but have provided more detailed microstructural evidence.

Such evidence has allowed the kinetic stages of OPC and C_3S hydration (as determined by calorimetric measurements [7] or calcium/silicate ion concentration in solution [29]) to be identified with specific reaction-product evolution. Also, a number of different C–S–H morphologies have been identified and documented. Various workers have proposed different schemes when detailing these types of C–S–H, but there seems to be little differentiation by the authors between the morphology of products formed from pure silicates and the more complex cement systems. The formation of C–S–H in OPC hydration is often thought of as an impurity perturbed case of C_2S and C_3S. This is reflected in a cross-correlation between studies performed on both materials, and is a further indication of the importance of the silicate components. For example, Lawrence and Young [27] and also Diamon *et al.* [13] prefer the "inner" and "outer" product description of C_3S hydration. This interpretation labels the initial gelatinous C–S–H product as being "inner" and the later inter-granular fibrillar C–S–H and crystalline CH as "outer". Double *et al.* [4] apply the same description to the C–S–H arising from OPC hydration and comment only briefly on the potential differences due to impurity. Brunauer and Greenberg [17] propose the formation of primary (initial C–S–H) and secondary products (later fibrillar C–S–H and CH) in the C_3S hydration process. They explain the radical morphology change as a "rolling up" of the initial "foil like" morphology. Diamond [30] extends the inner and outer product description to include four types of C–S–H. His sub-division is as follows.

Type I: fine fibrous network, formed in immature pastes after several hours.

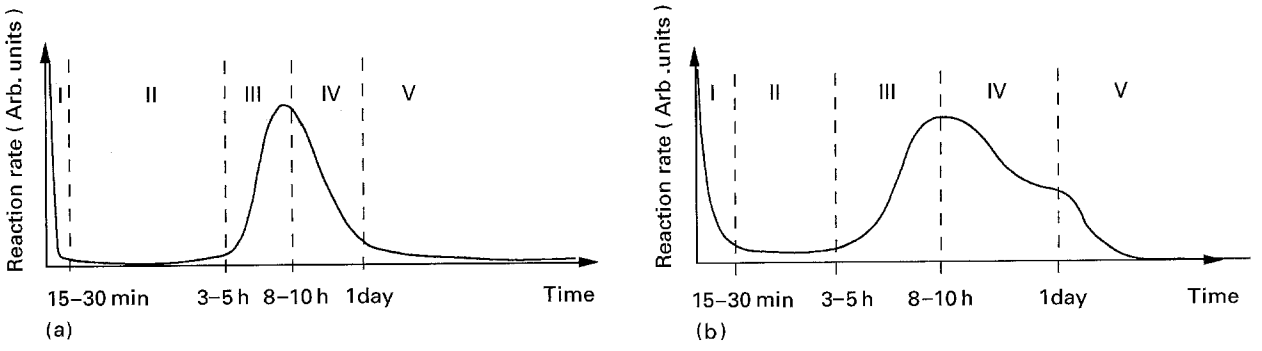

Figure 1 Schematic illustration of conduction calorimetry results showing the various stages of (a) OPC and (b) C_3S hydration (adapted from [3]).

Type II: reticular network of intersecting acicular particles formed in more mature pastes after many days.

Type III: continuous network filling the space between grains, formed in very mature pastes.

Type IV: fine-grained colloidal gelatinous "inner product" formed initially during stages 1 and 2.

Barnes *et al.* [22] further develop the multi-stage morphology idea by describing the products in terms of "Hadley grains". These consist of an anhydrous unreacted central core, surrounded by the gelatinous inner product (Type IV), and encapsulated in the fibrillar morphology of outer product (Types I–III).

1.3. "Wet" electron microscopies

Conventional electron microscopy has undoubtedly been extremely useful in extending our understanding of the hydration process. There are, however, significant problems with such techniques due to the fact that observation takes place under high vacuum. "Wet" specimens are notoriously difficult to deal with in this dehydrating environment. The possibility that a particular microstructural feature is merely an artefact of complicated and damaging preparation is always a worry. For example, traditional SEM sample preparation often involves procedures such as reaction quenching, complete sample drying, fracture to expose clean and typical surfaces, and coating with a conducting layer to prevent image distortion. Delicate samples, such as those indicative of early hydration studies ($t < 3$ h), are not self-supporting, and so techniques such as resin impregnation [19] and freeze drying have been employed [23]. TEM studies pose an additional problem of needing very thin samples, and so ion-beam milling and microtoming of hardened pastes has been used [28].

Attempts to limit the effects of such preparation techniques have included Cryo-SEM [5] and frozen hydrated SEM [21]. Not withstanding these efforts, the fact remains that microstructural evidence obtained from "dry" microscopy may contain artefacts. There are, however, a few isolated publications which detail microscopy studies of "wet" pastes. Notably, Double *et al.* [4] have used an environmental cell within a high-voltage TEM. They report observations of isolated grain reactions in high water-to-cement ratio mixtures. The cell thickness was restricted to ~ 20–50 μm, but significant electron scatter was still observed. This fact, coupled with the random movement of the grains, produced results that were not entirely unambiguous. Another example of such *in situ* hydration studies is found in the work of Jennings *et al.* [9]. They report the use of a gas reaction cell in high-resolution SEM and STEMs to observe the detailed morphology of C–S–H.

Currently, the potential for examining samples in a more-nearly natural state is expanding. So-called "natural", "wet", "low pressure" [31], or "environmental" SEM instruments are being used in a variety of applications where flexible observation conditions are required. Environmental SEM (ESEM) [32] is one of the more widely used of these specialist techniques. Samples are imaged in the presence of water vapour or some other auxiliary gas such as nitrogen. By differential pumping, the observation chamber can be held at pressures up to 25 torr (1 torr = 133.322 Pa), whilst the gun and column remain at 10^{-6}–10^{-7} torr. These gradients are manufactured by a series of pressure-limiting apertures (PLAs) and separate pumping units for each zone (Fig. 2). With short working distances (~ 2–5 mm) and gas pressures in the region 1–25 torr, a significant proportion of the electron beam is retained within the probe volume. Scattering in these circumstances is referred to as "oligo" (Fig. 3a) as opposed to plural (Fig. 3b) [33]. Conventional high-vacuum scintillation-based detectors cannot be used in such circumstances. The presence of a gas in the chamber is utilized in the so-called "environmental secondary" or "gaseous" detector (ESD/GD) [34]. A schematic drawing of this configuration is shown in Fig. 4. An electrode is biased with respect to the sample surface, and, depending on the magnitude and polarity of the resultant field, different charged species are accelerated through the gaseous environment. Cascade amplification of signal arising from the specimen yields high signal-to-noise ratio, and an image is reconstructed from the measured electrode current. The positive ions produced in this cascade process may then be used to neutralize excess negative charge

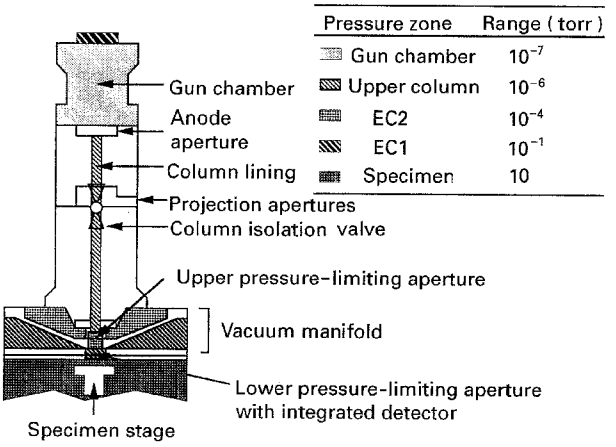

Figure 2 Schematic illustration of the Electroscan E-3 ESEM, demonstrating how differential pumping can be used to produce a pressure gradient from the gun to the specimen chamber.

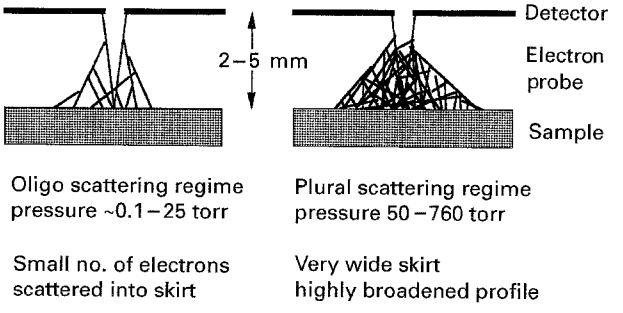

Figure 3 Electron-beam scattering in an environmental gas. At low pressures (0.1–25 torr), the oligo regime dominates, and only a small number of electrons are scattered out of the probe into the beam skirt. At higher pressures (50–760 torr), plural scattering occurs and the beam is heavily broadened.

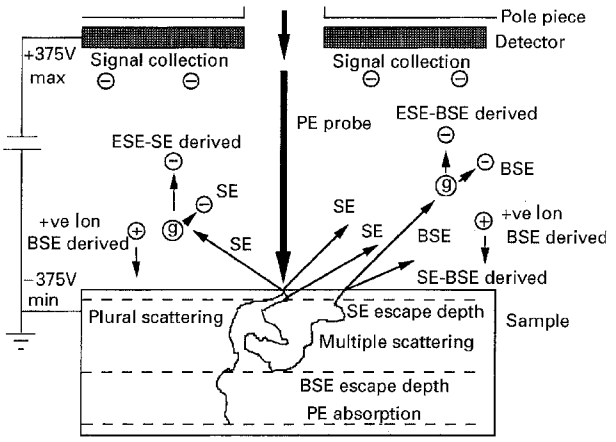

Figure 4 Operation of an environmental secondary detector (ESD) or gaseous detector (GD) in the Electroscan ESEM. Under conditions of negative sample bias, signal electrons from the specimen surface are accelerated to the detector, and undergo ionizing collisions. Particle type: SE, secondary electron; BSE, back scattered electron; ESE, environmental secondary electron; g, gas molecule.

that builds up to the sample surface. Hence, electrically insulating specimens do not need to be coated with a conducting layer in order to prevent image distortion.

By controlling the temperature of the sample, and using water vapour as the imaging gas, saturated conditions can be produced. Dehydration can be inhibited by the correct pump-down procedure [35], and wet samples can, therefore, be observed in their "natural state". This flexibility in observation environment also means that the structural changes associated with certain chemical reactions can be studied *in situ* and in real time. A comparative study of tricalcium silicate hydration results obtained using SEM and ESEM has been published by Bergstrom and Jennings [15]. Such "wet" electron microscopy literature is, however, very scarce.

In combining techniques, for example calorimetry and "wet" electron microscopy, extreme caution has to be exercised. The reaction kinetics, and hence the temporal evolution of products, is greatly influenced by a number of important experimental factors. These include:

(i) sample composition – for example, in C_3S different crystallinities and impurity levels can produce widely varying reactivities, (see a correlation between the results of Tadros *et al.* [29] Menetrier *et al.* [36] and Young *et al.* [37], published in Jawed *et al.* [6]);

(ii) reaction temperature – can affect the duration of each hydration stage, and the degree of hydration [4]; and finally

(iii) water-to-solid content – (w/s) of the mixture dictates the solute ion concentration, and so controls such critical factors as CH crystallization [4].

The calorimetry data presented here merely serve to indicate the temporal position of stages I, II, and III, allowing the direct microstructural evidence of ESEM to be interpreted within this kinetic sequence. In order that this correlation be valid, the hydration conditions in both sets of experiments were kept similar for some of the reasons just mentioned.

This paper seeks to illustrate that the "wet" microscopy technique of ESEM is a useful tool in the study of hydrated specimens. An experimental methodology will be outlined, in which the unique capabilities of ESEM are used to investigate the particular example of pre-induction and induction phenomena in C_3S. The results of these direct obervations are discussed in terms of popular hydration mechanism theories, and the previously mentioned ideas concerning C–S–H microstructure. Comments are also made in support of several OPC hydration mechanisms which rely intimately upon the C_3S component.

2. Experimental procedure

2.1. Materials

The tricalcium silicate samples used in both DSC and ESEM investigations were supplied by Construction Technology Laboratories (CTL), Skokie, IL, part no. TJC01. The powdered material (mesh 20) contained rough grains in the size range 1–100 μm. Chemical compositions were assessed using quantitative X-ray microanalysis in the ESEM. For this purpose, a Kevex SIGMA 2 system was used in conjunction with a Peltier cooled APD energy-dispersive X-ray detector. Several different samples were analysed in the presence of water vapour under the conditions shown in Table I. These characterizations proved that the C_3S contained a very low level of impurity. A typical composition is shown in Table II, this particular sample having 0.4% by atomic weight of iron.

C_3S is known to exist in a number of different polymorphs depending upon impurity content and temperature. These crystal structures were investigated by Jeffrey [38]. The trigonal pseudostructure that he proposed has proved to be a good approximation to the true structure [39]. Up to approximately 1100 °C, seven forms are known to exist, and these are designated as T_I, T_{II}, T_{III}, M_I, M_{II}, M_{III}, and R, where T, M, and R are triclinic, monoclinic, and trigonal, respectively. Transformation between the states involves tiny displacements of structural groups [40, 41]. At normal temperatures (< 600 °C), only the T_I phase is stable. However, the presence of impurity ions within the crystal lattice (magnesium, aluminum or transition

TABLE I The instrument conditions for ESEM X-ray microanalysis of C_3S

Beam current	1.0 pA	Gas pressure	5.0 torr
Beam voltage	20 kV	Tilt angle	0°
Work distance	10.1 mm	Take-off angle	15°

TABLE II The composition of a typical C_3S sample

Element	Line	Error	(at%)
O	K_a	0.2	78.1
Si	K_a	0.3	4.2
Ca	K_a	0.8	17.3
Fe	K_a	0.2	0.4

metal ions) may allow the other polymorphs to exist. In OPC, all structures are found, but monoclinic invariably dominates [42]. It is therefore surprising that the C–S–H morphology arising from the least prevalent triclinic (T) form best approximates the structure found in OPC [5].

To assess the crystallinity, and identify the particular polymorph of the sample, X-ray diffraction measurements were carried out at Schlumberger Cambridge Research (SCR). The results of this characterization indicated that the C_3S was of the triclinic form. This analysis was in agreement with the quantitative energy dispersive data provided by the Kevex system, which showed very low levels of impurity.

2.2. Environmental scanning electron microscopy observations

The "wet" capability of an Electroscan E-3 ESEM can be used in conjunction with temperature control to initiate, promote/retard, observe, and terminate the hydration reaction of tricalcium silicate. The underlying principle of the experimental technique is demonstrated by the plot of saturated vapour pressure versus temperature for water, shown in Fig. 5, but the exact experimental technique is as follows. The C_3S powdered sample was put in a copper pot ($\sim$ 50 µl capacity) and placed on the microscope Peltier stage at a temperature of $\sim$ 20 °C. The pumping sequence, as prescribed by Cameron and Donald [35], was carried out to maximize relative humidity, and an imaging pressure of $\sim$ 5.5 torr of water vapour set. The "dry" sample was then viewed under the conditions shown in Table III. The morphologies of these fresh grains were recorded for reference. The sample temperature was then reduced to $\sim$ 5–7 °C and, according to the data shown in Fig. 5, condensation of water on to the surface occurred. Two complementary hydration modes were employed from this stage on. In the first, designated methodology A, different samples were hydrated for periods varying from 30 s to 3 h. At the end of the designated times, excess surface water was removed by raising the stage temperature by $\sim$ 2 °C, allowing the C_3S microstructure to be recorded (conditions as shown in Table III). At this point, the grain surfaces were still partially hydrated, and as such the products remained in their natural state. Once satisfactory micrographs had been obtained, the sample was removed from the microscope, and replaced with fresh C_3S in preparation for the next hydration/partial dehydration sequences. The second technique, designated methodology B, employed the same method of producing condensation. However, the reaction of a single sample was followed by partially dehydrating its surface at various times during the process, and recording the microstructure. After each of these recording stages, condensation was promoted by reducing the temperature, once again fully hydrating the same sample. The resultant exposure in this case, therefore, consisted of a series of partial dehydrations and re-hydration sequences, the sample spending a total of 1 h in the wet state.

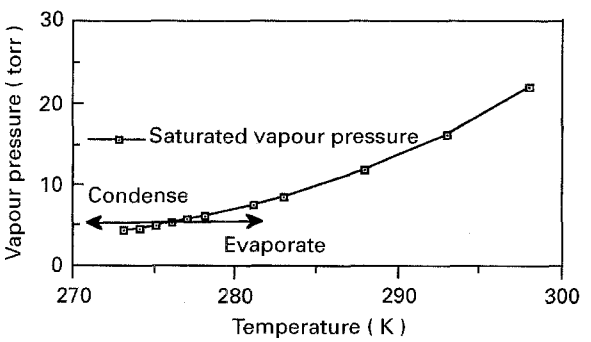

Figure 5 A plot of saturated vapour pressure of water versus temperature, demonstrating how the ESEM can be used for "wet" experiments.

TABLE III ESEM operating conditions during methodologies A and B

	Gun voltage (V)	Work dist. (mm)	Pressure (torr)	Temperature (°C)
"Dry"	25	7–12	5–5.5	20
"Wet"	25	7–12	5–5.5	8

In both methodologies, the samples were placed in thermally conducting copper pots. During the condensation stage, the C_3S was fully wetted by allowing the pot to fill with water. Following this procedure gave high water-to-solid ratios of $\sim$ 10:1. Such a regime has previously been used in "wet" electron microscopy work by Jennings *et al.* [9] and also Double *et al.* [4], and in "wet" optical microscopy performed by Diamon *et al.* [13]. Sufficient areas of sample were studied in both ESEM methods to ensure representative images were obtained. Also, for completeness, isolated grains (5–10 µm size) and clusters were observed.

Two alternative hydration schemes were investigated in order to assess the damage caused by continued partial dehydration and rehydration. It was thought that methodology A would be more reliable.

2.3. Differential scanning calorimetry measurements

The kinetics of hydration were studied using a Perkin–Elmer DSC 7 instrument, the operation of which is based upon a power-compensated "null" balance principle. The heat generated during a reaction is measured by adding or subtracting an equivalent amount of electrical energy from the sample in order to maintain a reference temperature. The DSC was operated in isothermal mode, and the following experimental procedure was used. Samples were prepared in 40 µl capacity DSC pans with water-to-solids (C_3S) ratio of $\sim$ 10:1. The pans were lidded and sealed before being weighed and rapidly transferred to the DSC chamber. Similar pans containing dry C_3S powder were used in the reference arm of the calorimeter. This was done to provide an approximate thermal match to the paste, and so reduce the time required to attain equilibrium after the ramp stage of

the programme. The specimens were loaded at 30 °C, before being cooled over a period of 1 min to the isothermal temperature of 8 °C. The amount of heat genererated over 4 h was then recorded. A dry C_3S specimen of the same weight was also scanned under identical conditions to the reacting mixture, in order to assess the instrumental response of the DSC. From these results, it was estimated that the first 4 min of the reaction were lost due to the loading procedure, and the uncertainty of pre-equilibrium data. Consequently, the zero point of the experiment was defined as the time from which data are deemed to be reliable.

3. Results

3.1. Environmental scanning electron microscopy

3.1.1. Methodology A

Apart from a small amount of texture, the surface structure of anhydrous C_3S grains was found to exhibit few features. The grains were irregularly shaped and highly polydisperse. A typical sample is shown in the electron micrograph of Fig. 6a. This grain is isolated and measures approximately 10 μm × 20 μm. When the C_3S grains were hydrated according to methodology A, a surface product was observed upon immediate contact with water. At early stages, for example after 1 min, the layer appeared irregular and discontinuous. This early change in morphology is demonstrated by the electron micrographs shown in Fig. 6a (dry grain) and b (wet grain). Hydration for longer times ($t < 20$ min) had the effect of propagating and thickening this layer, whilst not producing any inter-granular material.

Continued exposure up to ~ 20–30 min had the effect of further increasing the coating extent and thickness. Whole clusters of grains were seen to be completely draped in the product, and large pits on grain surfaces were covered and bridged by a self-supporting layer. A comparison between the grain surface at zero time, i.e. before hydration, and after 25 min is shown in Fig. 7a and b. The area on the centre left shows clearly how an originally isolated grain becomes engulfed by the covering material. Further structural evolution did not occur after hydration for ~ 30 min. However, the samples exposed for

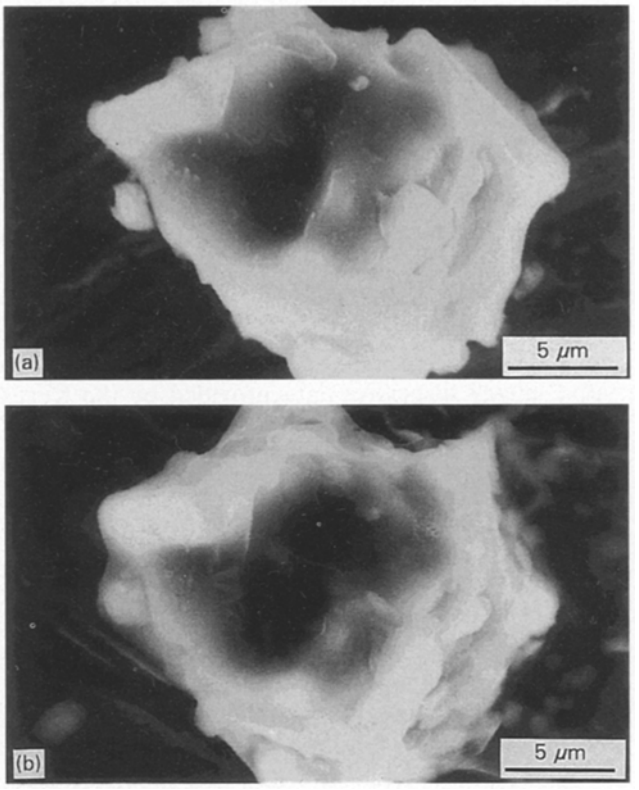

Figure 7 An ESEM electron micrograph showing (a) an isolated, dry grain of C_3S prior to hydration, and (b) the same grain after hydration by methodology A for 25 min, showing complete coverage of the surface by C–S–H.

~ 3 h displayed a dramatic change in morphology. Large, regular, hexagonal crystals could clearly be seen in inter-granular regions, and over the grain surfaces themselves. These crystals were in various degrees of development, but occurred throughout the samples. A clear example of such structures is shown in Fig. 8a (dry grain) and b (grain after 3 h hydration).

3.1.2. Methodology B

Upon hydration according to methodology B, once again, product was seen to form immediately at the grain surfaces. Initially, this consisted of a thin amorphous coating, which continued to grow and thicken with increased exposure. During the first

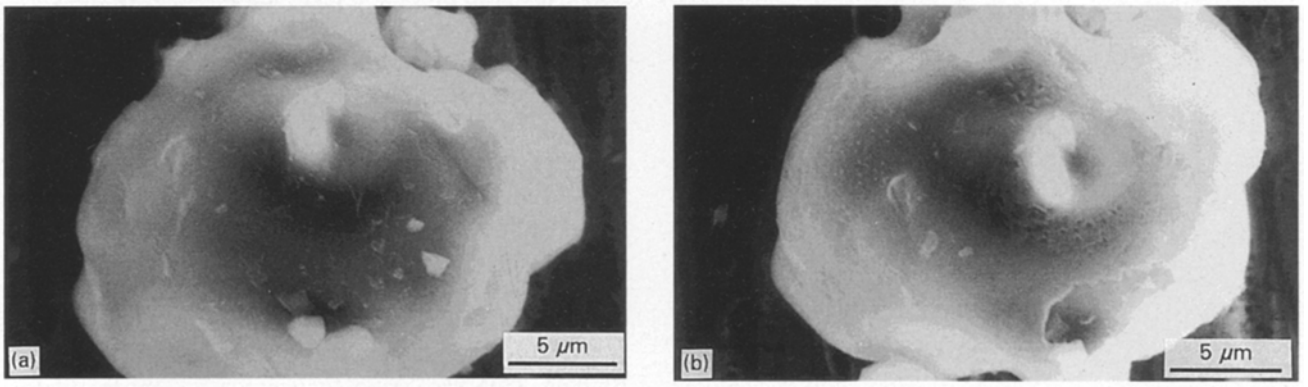

Figure 6 An ESEM electron micrograph showing (a) an isolated, dry grain of C_3S prior to hydration, and (b) the same grain after hydration by methodology A for 1 min, showing the very early formation of a C–S–H layer.

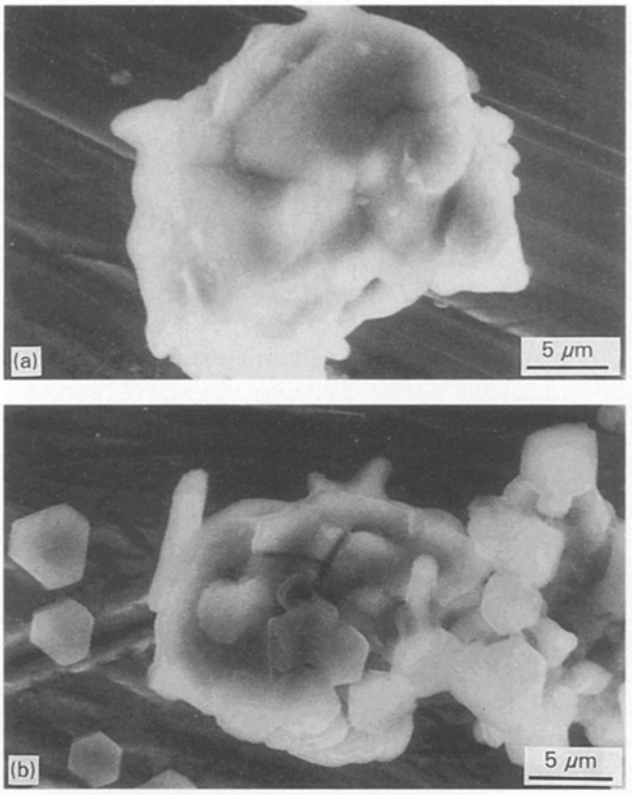

Figure 8 An ESEM electron micrograph showing (a) an isolated, dry grain of C_3S prior to hydration, and (b) the same grain after hydration by methodology A for 3 h, showing the formation of large, regular CH crystallites.

minutes of the process, no outer product, i.e. material between grains, was seen to develop. After approximately 7 min, having undergone 4 dehydration/re-hydration sequences, this situation changed dramatically. Although an extensive gelatinous surface coating continued to form, small irregular crystallites were seen in inter-granular areas. Such structures are demonstrated in the electron micrograph of Fig. 9b, when viewed in comparison with the dry grain of Fig. 9a.

Continued exposure failed to cause the crystals to propagate any further, and in most cases their size and occurrence regularity both reduced. However, the grain coatings thickened and grew throughout the exposure. An example of the extent of surface coverage that was evident after 25 min is shown in Fig. 9c. After this time, the products (inner and outer) ceased to evolve any further.

3.2. Differential scanning calorimetry

Results obtained from the differential scanning calorimeter studies indicated that, as expected, there were three distinct stages to the reaction. For the high water-to-solid mixtures used in these experiments, the end of stage 1 corresponded to a total hydration of between 25 and 35 min. Stage 2 induction, as characterized by a marked decrease in activity, was found to last for a further 150 min (approximately). After this period, the reaction was observed to proceed once more, indicating the onset of stage 3. An example of this sequence is shown in Fig. 10a (pre-induction and early induction), and b (induction and post-induction)

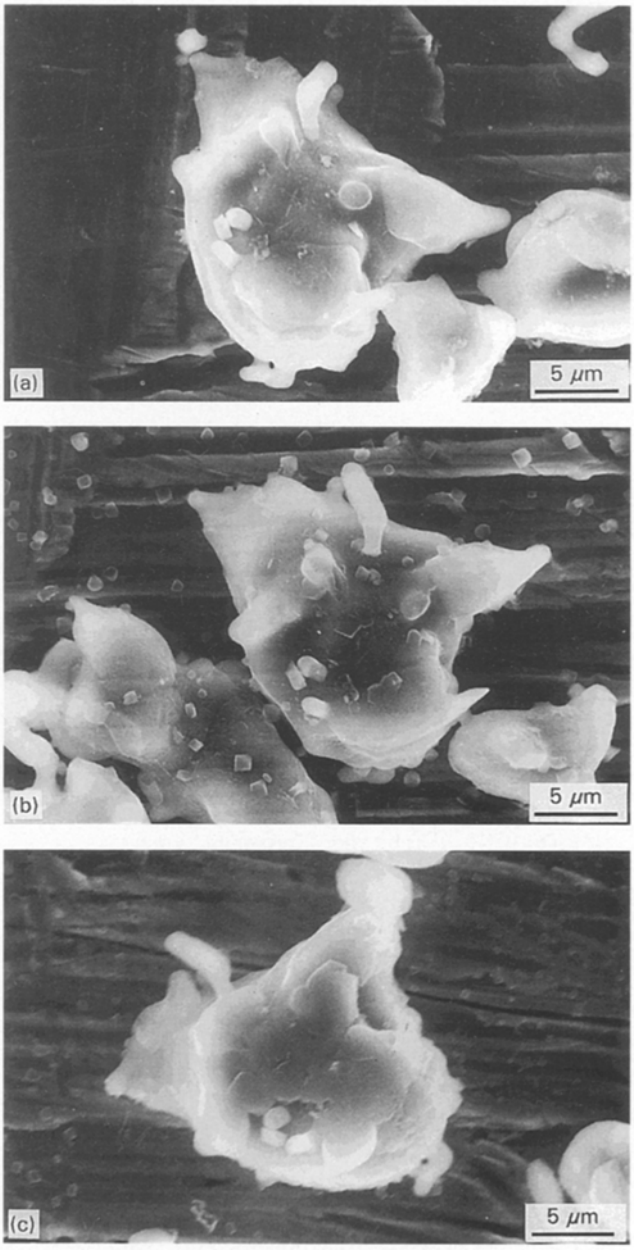

Figure 9 An ESEM electron micrograph showing (a) an isolated, dry grain of C_3S prior to hydration, and the same grain after hydration by methodology B for (b) 7 min, and (c) 25 min, showing the development of microstructure.

for the same sample. These data have been normalized with respect to the first reliable values obtained at the beginning of the experiment (stage 1), in order to provide a sensible scaling for the entire reaction. It is important to note that the most highly exothermic portion of the hydration (the initial dissolution of ions) falls within the loading time and pre-equilibrium part of the procedure, and that all subsequent phenomenological assignments are relative to the "zero point". The transitions between stages 1, 2 and 3 have been approximately marked on Fig. 10, and provide a temporal benchmark for the following discussion.

4. Discussion

In the following section, the above results will be discussed within the framework of "accepted" C_3S hydration theories. This discussion will be logically

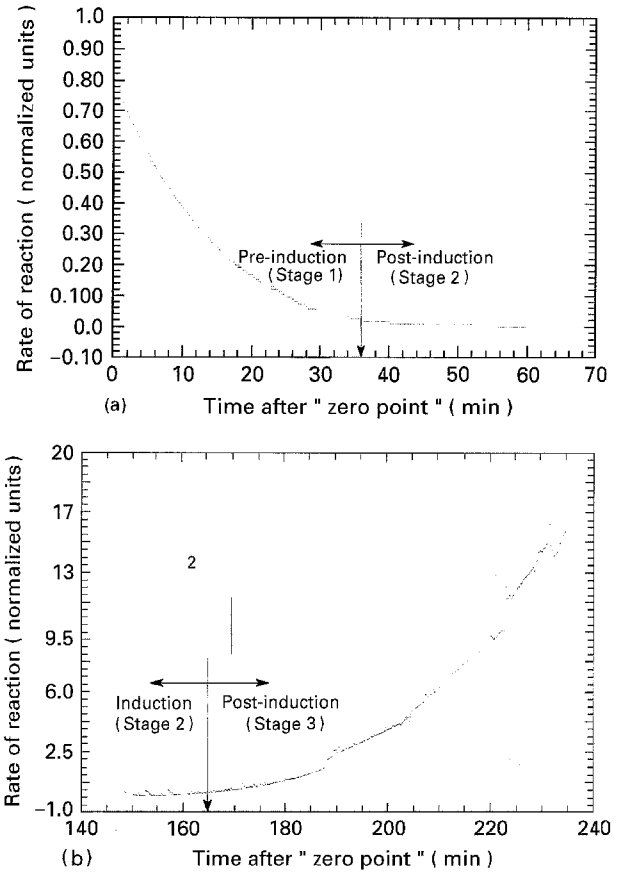

Figure 10 Results of DSC measurements on a water-to-solid ratio of ~ 10:1 sample of C_3S paste, rate of reaction (normalized with respect to the first reliable data point) as a function of time, showing: (a) stage 1, as characterized by the initial exothermic reaction, terminating after ~ 25–35 min, followed by the inactive dormant stage 2 period, and (b) this dormancy terminating after ~ 3 h and the rate of reaction rising once more, marking the onset of stage 3.

split into pre-induction (stage 1) and induction (stage 2) product evolution. In assigning the duration of, and transition between the stages, direct comparison will be made between microstructural and DSC data. As such, only qualitative comparison can be made between these results and those published by other authors on a variety of C_3S systems. One further point to note when considering this discussion, is that no attempt will be made to explain the stage 2 and 3 transition, i.e. the end of induction, or the evolution of fibrillar Type II and III product.

4.1. Pre-induction (stage 1) product evolution

Both sets of ESEM experiments showed that a coating formed over the grain surfaces immediately upon contact. This material displayed very little distinct structure or crystallinity on the resolution scale of the instrument (~ 20 nm under these conditions). This primary [17], inner [27], or Type IV [30] product is known to be C–S–H in its early morphological form [43]. The C–S–H layer was seen to thicken and extend to cover most of the grain surface by the end of stage 1 (as defined in the DSC results by a drop in the reaction rate), after which time no further growth was noted.

The reaction of C_3S with water proceeds as previously discussed via the approximate route of Equation 1. Calcium ions are rapidly released into solution during the very early moments of hydration [6]. The pH of the solution rises to ~ 12 after a few minutes [3]. However, the dissolution of silicate ions is not as dramatic [29], and the resultant C–S–H surface product is, therefore, silicate-rich. The ESEM evidence suggests that continued extension of this layer can occur until the entire surface of the grain has been covered. Hence, it is postulated that the beginning of C_3S induction is associated with the exhaustion of easily available surface reactants. The rate of reaction is known to be critically dependent upon water-to-solid ratio and temperature [4]. Therefore, it is consistent that this exhaustion point varies according to hydration conditions and sample composition [6].

4.2. Induction (stage 2) product evolution

As previously mentioned, the development and growth of surface C–S–H ceases at the end of stage 1. Kinetically, this corresponds to a dramatic reduction in the reaction rate. This dormancy lasts until the beginning of stage 3, as denoted by increased activity once more. At this point, our methodology A results clearly showed that large regular hexagonal crystals appeared. Such a structure is known to be associated with CH formed as a result of nucleation and growth from saturated or supersaturated calcium solution [44]. The reason for the premature appearance of CH much earlier in the methodology B results will be explained later.

The presence of CH product has been noted in mature OPC pastes by other workers. For example, Lawrence and Young [27] observed large crystals in pores of etched samples. However, direct microstructural evidence for CH formation at the end of induction is rare.

Measurements of calcium and silicate-ion concentrations during stages 1–3 have yielded such a correlation. Slegers and Rouxhet [45] used a calcium-sensitive membrane electrode to follow calcium concentration during hydration. They found that the observed super-saturation peak corresponded to increased activity at the beginning of stage 3. It has also been observed [29] that after the initial burst of dissolution during stage 1, both calcium- and silicate-ion concentrations gradually increase throughout stage 2. This, therefore, suggests a mechanism by which a critical ion concentration builds up during induction, reaching the necessary levels at the end of stage 2, and causing crystallization of CH. Such a clock reaction type process has, in fact, already been suggested by Billingham and Coveney [46], to explain the reaction of C_3A and gypsum to produce ettringite during OPC hydration.

The critical ion concentration theory for CH formation is supported by some of the methodology B results. Small, irregular crystallites were seen prematurely during stage 1. This different experimental technique had the consequence of artificially promoting the local calcium ion concentration by the

successive dehydration and re-hydration sequences. A similar premature crystallization was noted by Slegers and Rouxhet [45] in their membrane electrode experiments. They also observed smaller, less regular crystals (in comparison to the later stage 2/3 product), and explained the phenomena by localized impurity sites providing lower nucleation potentials.

The continued increase in calcium-ion concentration in solution during induction is critically dependent upon the microstructure of the protective C–S–H layer that forms. During this period, anhydrous C_3S must continue to hydrate in order for this to occur. Calorimetry data indicate that this happens at a much reduced level during stage 2, because the rate of reaction is significantly lower. However, the exact structural nature of the C–S–H coating is a matter of uncertainty. The critical question as far as the continued limited stage 2 hydration of C_3S is concerned, is whether this coating is impermeable, semi-permeable or porous to water. A commonly accepted "generic" interpretation of the structure of C–S–H is based upon a so-called "degenerate clay" model [47–50]. This form implies a randomly arranged bread-and-butter layered structure in which sheets of hydrated calcium silicate (bread) are separated by a filling of water and calcium ions. If a protective layer of amorphous C–S–H were to form on the grain surface (as indicated by the ESEM results), it would allow for the through-transport of both hydrate and calcium ions by an osmotic mechanism [4]. This structure does not, therefore, preclude the critical ion concentration argument for later precipitation of crystalline calcium hydroxide. A schematic illustration of this idealization is shown in Fig. 11.

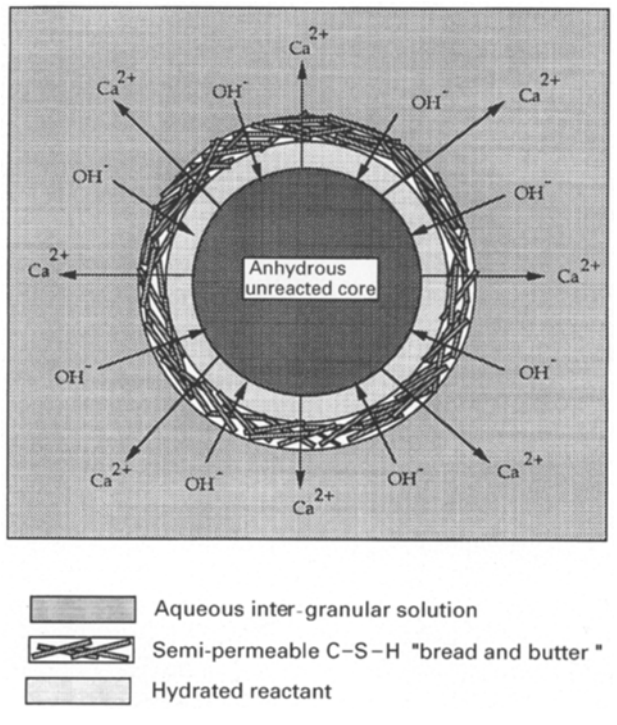

Figure 11 An idealized schematic illustration of the stage 1 pre-induction and stage 2 induction hydration of C_3S, based upon a protective layer topochemical mechanism for the reaction.

5. Conclusion

This paper has detailed an electron microscopy technique for directly studying morphology evolution in tricalcium silicate during very early induction and pre-induction hydration. ESEM results have been presented which indicate the initial development of hydrated calcium silicate gel, and the post-induction (as indicated by the DSC data) formation of crystalline calcium hydroxide products. ESEM evidence supports the hypothesis that stage 2 is characterized by microstructural inactivity. This was confirmed by calorimetric information, which indicated that the reaction rate was very low during the induction phase of the process.

Comparison between the results obtained by methodology A and methodology B, demonstrate that the correct experimental procedure is essential. By slight modifications to method A, artificially high concentrations of calcium ions could be manufactured in technique B. This was seen by the early formation of small calcium hydroxide crystals during stage 1, as opposed to the end of induction (methodology A). Both results support the critical ion hypothesis for CH crystallization.

All the ESEM observations have been integrated within an adapted protective-layer topochemical mechanism for the early pre-induction and induction hydration of C_3S, the main points of which are:

(a) early stage 1: an initial dissolution of calcium and silicate ions into solution, accompanied by a rapid reaction rate and the immediate formation of a protective C–S–H grain coating (inner or type IV product);

(b) mid-stage 1: increased coverage of the grain surfaces by C–S–H, and the continued dissolution of ions, accompanied by a drop in the reaction rate;

(c) late stage 1: a complete coverage of the grain surface, inhibiting further access to unreacted anhydrous C_3S and layer growth, with an associated fall in reaction rate to induction levels;

(d) mid-stage 2: continued dissolution of calcium ions from unreacted buried grain surfaces and pores, enabled by osmotic transport through the C–S–H membrane;

(e) late stage 2: the achievement of a critical calcium concentration in solution leading to nucleation and growth of CH crystals, and an accompanying continuation of C–S–H outer product formation.

The use of "wet" electron microscopy techniques has been shown in this paper to have distinct advantages over conventional dry, *post mortem* analysis. Firstly, the need for complicated preparation techniques prior to analysis has been removed. Consequently, the artefact concerns arising from such procedures have been eliminated. In addition to these facts, ESEM has allowed the actual reaction to be dynamically controlled *in situ* and for the process to be studied in real-time. Finally the technique has enabled the very early pre-induction hydration phenomena to be observed. Future work will involve the study of post-induction phenomena in C_3S, and the application of the technique to C_3A, C_4AF and OPC hydration.

Acknowledgements

This work was performed in collaboration with Schlumberger Cambridge Research, and was funded under the Colloid Technology Programme by the Department of Trade and Industry, Unilever, Zeneca, ICI, and Schlumberger. The authors thank Mr Andrew Eddy, Cavendish Laboratory, for his contribution to the ESEM studies.

References

1. H. F. W. TAYLOR, "Chemistry of Cements" (Academic Press, London, 1990) p. 123.
2. G. C. BYE, in "Portland Cement, Composition, Production and Properties" (Pergamon, Oxford, 1983) p. 90.
3. S. MINDESS and J. F. YOUNG, in "Concrete" (Prentice-Hall, NJ, 1981) p. 86.
4. D. D. DOUBLE, A. HELLAWELL and S. J. PERRY, *Proc. R. Soc. Lond.* **A359** (1978) 435.
5. H. R. STEWART and J. E. BAILEY, *J. Mater. Sci.* **18** (1983) 3686.
6. I. JAWED, J. SKALNY and J. F. YOUNG, in "Structure and Performance of Cements", edited by P. Barnes (Applied Science, London, 1983) p. 237.
7. J. A. FORRESTER, *Cem. Technol.* (May) (1970) 95.
8. P. L. PRATT and A. GHOSE, *Phil. Trans. R. Soc. Lond.* **A310** (1983) 93.
9. H. M. JENNINGS, B. J. DALGLEISH and P. L. PRATT, *J. Amer. Ceram. Soc.* **64**(10) (1981) 567.
10. R. KONDU and S. UEDA, in "Proceedings of the Fifth International Symposium on the Chemistry of Cements", The Cement Association of Japan, Tokyo (1968), Vol. II.
11. W. MICHAELIS, *Kollid Z.***5** (1909) 9.
12. W. C. HANSEN, in "Proceedings of the Third International Symposium on the Chemistry of Cements", Cement and Concrete Association, London (1952).
13. M. DIAMON, S. UEDA and R. KONDE, *Cem. Concr. Res.* **1** (1971) 391.
14. N. L. THOMAS and D. D. DOUBLE, *ibid.* **11** (1981) 675.
15. T. B. BERGSTROM and H. M. JENNINGS, *J. Mat. Sci. Lett.* **11** (1992) 1620.
16. J. D. BIRCHALL, A. J. HOWARD and D. D. DOUBLE, *Cem. Conc. Res.* **10** (1980) 145.
17. S. BRUNAUER and S. A. GREENBERG, in "Proceedings of the Fourth International Symposium on the Chemistry of Cements", Washington (1960) (N. B. S. Monograph 43, Vol. I (1962) 135).
18. M. COLLEPARDI and B. MARCHESE, *Cem. Concr. Res.* **2** (1972) 57.
19. M. S. STUCKE and A. J. MAJUNDER, *ibid.* **7** (1977) 711.
20. I. ODLER and H. DORR, *ibid.* **9** (1979) 239.
21. P. J. M. MONTEIRO, S. J. BASTACKY and T. L. HAYES, *ibid.* **15** (1985) 687.
22. B. D. BARNES, S. DIAMOND and W. L. DOLCH, *ibid.* **8** (1978) 263.
23. D. M. F. ORR, *ibid.* **13** (1983) 146.
24. S. CHATTERJI and J. W. JEFFERY, *Nature* **209** (1966) 1233.
25. G. W. GROVES, *Cem. Concr. Res.* **11** (1981) 713.
26. H. M. JENNINGS and P. L. PRATT, *ibid.* **9** (1979) 501.
27. F. V. LAWRENCE and J. R. YOUNG, *ibid.* **3** (1973) 149.
28. B. J. DALGLEISH and K. IBE, *ibid.* **11** (1981) 729.
29. M. TADROS, J. SKALNY and R. S. KALYONCEU, *J. Amer. Ceram. Soc.* **9** (1976) 344.
30. S. DIAMOND, *Cem. Concr. Res.* **2** (1972) 617.
31. A. N. FARLEY and J. S. SHAH, *J. Microsc.* **162** (1991) 107.
32. G. D. DANILATOS, *Microsc. Res. Technol.* **25** (1993) 529.
33. *Idem, Adv. Electronics Electron Phys.* **71** (1988) 109.
34. *Idem, Micron Microscopia Acta* **14** (1983) 307.
35. R. E. CAMERON and A. M. DONALD. *J. Microsc.* **173** (1994) 227.
36. D. MENETRIER, I. JAWED, T. S. SUN and J. P. SKALNY, *Cem. Concr. Res.* **9** (1979) 473.
37. J. F. YOUNG, H. S. TONG and R. L. BERGER, *J. Am. Ceram. Soc.* **60** (1977) 344.
38. J. W. JEFFREY, *Acta Crystallogr.* **5** (1952) 26.
39. N. I. GOLOVASTIKOV, R. G. MATEEVA and N. B. BELOV, *Kristallogr.* **20** (1975) 721.
40. I. MAKI and S. CHROMY, *Chem. Concr. Res.* **8** (1978) 408.
41. M. REGOURD, *Bull. Soc. Fr. Mineral Crist.* **87** (1964) 241.
42. P. GOURDIN, E. DEMOULIAN, F. HAWTHORN and C. VERNET, in "Proceedings of the Seventh International Congress on the Chemistry of Cements". Paris Editions Septima, Paris (1980).
43. A. GRUMEDO, in "Proceedings of the Fourth International Symposium on the Chemistry of Cements", Washington (1960) (N. B. S. Monograph 43, Vol. II (1962) 648).
44. R. B. WILLIAMSON, *Prog. Mater. Sci.* **15** (1972) 3.
45. P. A. SLEGERS and P. A. ROUXHET, *Cem. Concr. Res.* **7** (1977) 31.
46. J. BILLINGHAM and P. V. COVENEY, *J. Chem. Soc. Farad. Trans.* **89** (1993) 3021.
47. T. C. POWERS, "The Physical Structure and Engineering Properties of Concrete" Portland Cement Association, Skokie, IL Bulletin **90** (1958).
48. S. BRUHAUER, *Am. Sci.* **50** (1962) 210.
49. R. F. FELDMAN and P. J. SEREDA, *Eng. J. (Canada)* **53** (1970) 53.
50. F. H. WITTMAN "Cement Production and Use", 79-08 (Engineering Foundation, New York, 1979) p. 143.

Received 9 August
and accepted 31 October 1994